

Research Article

Open Access



T-S fuzzy-model-based adaptive cruise control for longitudinal car-following considering vehicle lateral stability

Changzhu Zhang, Xiaoyu Wei, Zhuping Wang, Hao Zhang, Xuyang Guo

Department of Control Science and Engineering, Tongji University, Shanghai 200092, China.

Correspondence to: Prof. Hao Zhang, Department of Control Science and Engineering, Tongji University, Shanghai 200092, China. E-mail: zhang_hao@tongji.edu.cn; ORCID: 0000-0002-4527-9610

How to cite this article: Zhang C, Wei X, Wang Z, Zhang H, Guo X. T-S fuzzy-model-based adaptive cruise control for longitudinal car-following considering vehicle lateral stability. *Intell Robot* 2022;2(4):371-90.<http://dx.doi.org/10.20517/ir.2022.26>

Received: 13 Aug 2022 **First Decision:** 29 Aug 2022 **Revised:** 27 Sep 2022 **Accepted:** 30 Sep 2022 **Published:** 7 Nov 2022

Academic Editor: Simon X. Yang **Copy Editor:** Jia-Xin Zhang **Production Editor:** Jia-Xin Zhang

Abstract

Adaptive cruise control is one of the essential technologies of advanced driver assistance systems, which is used to maintain a safe distance between an ego vehicle and a preceding vehicle and has been extensively applied in the automotive industry and control community. Note that some vehicle manoeuvres may approach handling limits to prevent collisions under complex road conditions, which often leads to vehicle lateral instability while cruising. In this study, a T-S fuzzy model predictive control framework is applied to the problem of adaptive cruise control. Variations in the preceding vehicle velocity and road surface conditions are considered to formulate adaptive cruise control as a tracking control problem of a T-S fuzzy system subject to parameter uncertainties and external persistent perturbations. Then, a robust positively invariant set is introduced to derive an admissible T-S fuzzy controller by solving a min-max optimization problem under a series of linear matrix inequality constraints. Finally, a CarSim/MATLAB joint simulation is conducted to illustrate the effectiveness of the proposed method, which ensures longitudinal adaptive cruise control for a car-following scenario with lateral vehicle stability.

Keywords: Adaptive cruise control, T-S fuzzy model predictive control, robust positively invariant set, lateral stability



© The Author(s) 2021. **Open Access** This article is licensed under a Creative Commons Attribution 4.0 International License (<https://creativecommons.org/licenses/by/4.0/>), which permits unrestricted use, sharing, adaptation, distribution and reproduction in any medium or format, for any purpose, even commercially, as long as you give appropriate credit to the original author(s) and the source, provide a link to the Creative Commons license, and indicate if changes were made.



1. INTRODUCTION

Advanced driver assistance systems (ADASs) play a critical role in the automobile industry^[1] by significantly decreasing drivers' workload while considerably improving driving safety and comfort^[2-5]. A few examples of common applications of ADASs in automobiles in recent years are lane-keeping assist (LKA), adaptive cruise control (ACC), electronic stability control (ESC), and the precrash system (PCS)^[6]. The ACC system is one of the first ADAS technologies for maintaining a safe distance between an ego car and a preceding vehicle^[7]. Radar sensors detect the velocity of the preceding vehicle, which the ACC system uses to automatically modify the speed of the driving vehicle by managing the throttle opening or brake pedal levels^[8].

Many adaptive cruise control strategies can be found in the literature to achieve longitudinal car-following and enhance driving performance. A fuzzy logic control technique is described in Ref.^[9] that executes the ACC function on an AIT intelligent vehicle using the distance error and relative velocity information. In Ref.^[10], a control system is presented that decreases vehicle waiting time at stop lights, as well as fuel consumption, by utilizing upcoming traffic signal information and short-range radar for optimal velocity trajectory planning. In Ref.^[11], a safe and comfortable longitudinal automation system with a human-in-the-loop strategy is integrated into an ACC system. In Ref.^[12], the use of a longitudinal controller for a smart and green ACC system is investigated to minimize energy expenditure and maximize energy regeneration.

Model predictive control (MPC) is a traditional control approach with demonstrated utility for solving multiobjective optimization problems under a variety of system constraints^[13,14]. In the past few years, MPC has been widely applied to the design of ACC systems. A few examples are presented here: in Ref.^[15], MPC is applied to the design of spacing-control laws for transitional vehicle manoeuvres. A fuel economy-oriented ACC system is developed in Ref.^[16] to minimize vehicle fuel consumption, and a generic scale reduction framework is formulated to alleviate computational loads induced by the MPC optimization solution. In Ref.^[17], a benchmark setting for the MPC on a piecewise affine system is presented for the design of ACC algorithms, and different methods are implemented and evaluated to assess their main attributes, characteristics, and strong/weak points. A stochastic MPC approach for minimizing vehicle fuel consumption is investigated in Ref.^[18]. An MPC method for increasing vehicle tracking accuracy and reducing fuel consumption is developed^[19] by taking into account external road information, spatiotemporal constraints and nonlinear powertrain dynamics. In Ref.^[20], a personalized ACC system based on driving style identification is proposed to accommodate various driving types within an MPC framework.

The Takagi-Sugeno (T-S) fuzzy system consists of a cluster of linear subsystems as an approximation for a nonlinear system. Extensive studies have been performed on this system in recent decades^[21-24]. In vehicle control, vehicle dynamics are typically regarded as linear parameter varying (LPV) systems because of inevitable variations in parameters, such as longitudinal and lateral velocities. T-S fuzzy systems are constructed to model the vehicle dynamics and address parameter variations in the system. For example, in Ref.^[25], a fuzzy path-tracking controller is designed considering uncertain lateral tire forces, a time-varying vehicle speed, steering-input saturation and vehicle state conditions. In Ref.^[26], a fuzzy-model-based \mathcal{H}_∞ control algorithm is proposed considering constraints on the amplitude and rate of steering. In Ref.^[27], a path tracking controller based on output feedback is developed considering the transient behaviour of the system. However, few studies have been performed on integrating T-S fuzzy modelling into ACC systems, and this subject requires further investigation.

The aforementioned literature review shows that substantial progress has been made in both theoretical formulations and practical applications of ACC design for car-following within the model-based predictive control framework. Notably, cars may lose lateral stability when employing a cruise controller in some emergency situations, such as rapid braking on roads with low friction coefficients. Thus, vehicle lateral stability needs to be considered when developing ACC strategies. In some studies, a linear force relationship is utilized between

tires and roads, which does not precisely describe the lateral dynamical characteristics involved, leading to severe degradation or even instability of a closed-loop system, especially when a vehicle travels at high acceleration. The longitudinal velocity is intrinsically time-varying but is regarded as a constant in a few studies, which should also be addressed. The present study has been motivated by all these considerations.

The problem of adaptive cruise control design for longitudinal car-following considering vehicle lateral stability is investigated in this study. Vehicle longitudinal car-following kinematics are used in conjunction with two degrees-of-freedom vehicle lateral dynamics to formulate an adaptive cruise control system as a robust tracking control problem of a T-S fuzzy system by considering real-time variations of the velocity of the preceding vehicle. The corresponding control problem is then transformed into a min-max optimization problem within the T-S fuzzy control framework. The concept of robust positively invariant sets is introduced to effectively address some external norm-bounded disturbances, such as the steering angle of the front wheel and the acceleration of the preceding vehicle, to ensure that the states of the closed-loop tracking dynamics converge to a compact set. Finally, results of simulations using the CarSim/MATLAB joint platform are presented to demonstrate the effectiveness of using the proposed adaptive cruise controller to realize longitudinal car-following while ensuring vehicle lateral stability.

The main contributions of this study are as follows:

- (1) a T-S fuzzy control framework is used to first establish a unified T-S fuzzy dynamical model for car-following based on a combination of longitudinal kinematics, lateral dynamics, time-varying vehicle velocity, and non-linear lateral tire/road forces as a basis for designing adaptive cruise control;
- (2) a method is proposed for designing a coordinated controller of an adaptive cruise control system and a direct yaw moment control system that ensures simultaneous vehicle longitudinal car-following and lateral stability;
- (3) the developed controller design method is validated by tests in a high-fidelity CarSim/Simulink joint simulation environment, and the results clearly show the effectiveness of the T-S fuzzy model predictive controller and its superiority over a conventional controller design process that does not consider vehicle lateral stabilization.

The remainder of this paper is organized as follows. A mathematical model for a vehicle is presented in Section II, which includes longitudinal kinematics, lateral dynamics, and a tire/road force model. A design for a robust T-S fuzzy model predictive controller is presented in Section III. In Section IV, the lower layer of the designed adaptive cruise control algorithm is described. The CarSim/Simulink joint simulation results are presented in Section V. Finally, we conclude the paper in Section VI.

Notations and definitions: The notations used throughout this paper are quite standard. For any x in \mathbb{R}^n , x^T is its transpose and $|x|$ its Euclidean norm. For a $n \times m$ matrix A , $\|A\|$ stands for its induced matrix norm. \mathbb{Z}_+ denotes the set of all nonnegative integers. We use an asterisk “*” to represent a term that is induced by symmetry in symmetric matrices. A real-value function $\Phi : \mathbb{R}_{\geq 0} \rightarrow \mathbb{R}_{\geq 0}$ is a \mathcal{K} -function if it is continuous, strictly increasing, and $\Phi(0) = 0$; it is a \mathcal{K}_∞ -function if it is a \mathcal{K} -function and when $s \rightarrow \infty$, $\Phi(s) \rightarrow \infty$. A function $\beta : \mathbb{R}_{\geq 0} \times \mathbb{R}_{\geq 0} \rightarrow \mathbb{R}_{\geq 0}$ is a \mathcal{KL} -function if, for each fixed $k \geq 0$, $\Phi(\cdot, k)$ is a \mathcal{K} -function, and for each fixed $s \geq 0$, $\Phi(s, \cdot)$ is decreasing and $\Phi(s, k) \rightarrow 0$ as $k \rightarrow \infty$.

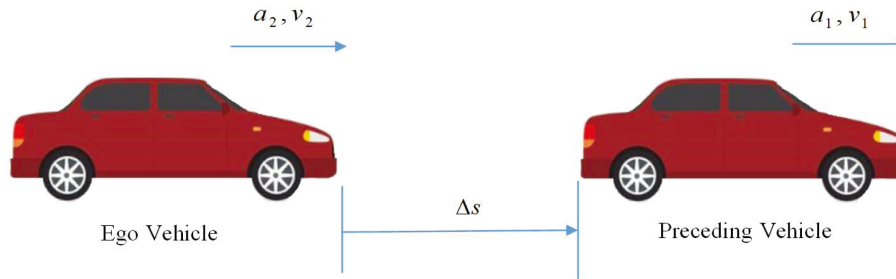


Figure 1. Vehicle longitudinal kinematics.

2. METHODS

2.1. Vehicle longitudinal kinematic model

The following symbols are used in the car-following situation shown in Figure 1: Δs is the distance between the preceding and ego vehicles; v_1 and v_2 are the longitudinal velocities of the preceding and ego vehicles, respectively; and a_1 and a_2 are the corresponding longitudinal accelerations.

The desired spacing distance between the preceding and ego vehicles is given as follows^[28]:

$$d_{\text{des}} = d_0 + t_0 v_2, \quad (1)$$

where d_0 is vehicle desired distance at standstill and t_0 is the constant headway time.

The difference in the desired and actual distances between the vehicles is defined as Δd , and the relative velocity between the preceding and ego vehicles is defined as Δv ; then,

$$\Delta d = \Delta s - d_{\text{des}}, \quad (2)$$

$$\Delta v = v_1 - v_2. \quad (3)$$

Considering the time delay of the engine in the driving system, we employ a first-order system to relate the actual vehicle longitudinal acceleration a_2 and the desired acceleration a_{des} as follows^[29]:

$$a_2 = \frac{1}{1 + \tau_0 s} a_{\text{des}}, \quad (4)$$

where τ_0 is the engine time constant, and a_{des} is the acceleration to be determined.

The definitions given above are used to express the vehicle longitudinal kinematic model as follows:

$$\begin{cases} \dot{\Delta d} = \Delta v - t_0 a_2 \\ \dot{\Delta v} = -a_2 + a_1 \\ \dot{a}_2 = \frac{-a_2 + a_{\text{des}}}{\tau_0} \end{cases} \quad (5)$$

2.2. Vehicle lateral dynamics

Figure 2 shows the classical two-degree-of-freedom (2-DOF) bicycle model of vehicle dynamics, which is simplified in this study by collapsing each axle to a single tire to reflect the fundamental features of lateral motions.

The mass of the ego vehicle is m . I_z is the moment of inertia about the yaw axis through the vehicle's centre of gravity (CG). l_f and l_r represent the distances from the vehicle centre to the front and rear axles of the vehicle, respectively. F_{yf} and F_{yr} denote the lateral forces on the vehicle front and rear tires, respectively. δ

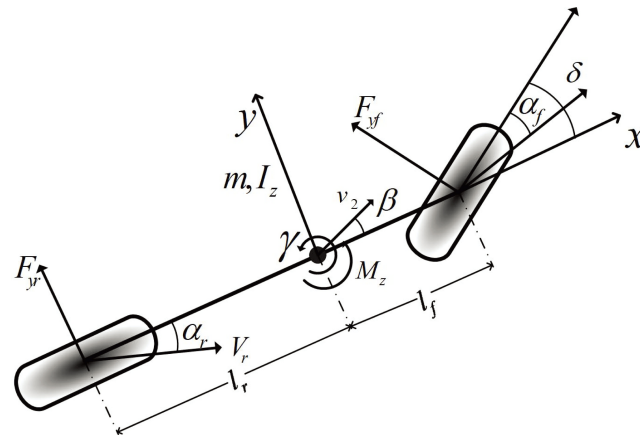


Figure 2. 2-DOF vehicle lateral dynamics.

is the steering angle for the front wheel of the vehicle. β , γ and v_x represent the sideslip angle, yaw rate, and longitudinal velocity of the ego vehicle, respectively. The vehicle lateral dynamics can be described in terms of the sideslip angle and yaw rate as follows:

$$\begin{cases} m v_2 \dot{\beta}(t) = F_{y_f}(t) + F_{y_r}(t) - m v_2 \gamma(t) \\ I_z \dot{\gamma}(t) = l_f F_{y_f}(t) - l_r F_{y_r}(t) + M_z(t) \end{cases} \quad (6)$$

where M_z is the external yaw moment generated by the differences in the longitudinal tire/road forces among the four tires of the vehicle.

2.3. Tire/road force model

The vehicle lateral tire/road force is generated by contact between the vehicle tires and the road surface^[30]. A tire operates in the linear region for a small vehicle lateral acceleration, which can be characterized by the cornering stiffness of the front and rear tires C_f and C_r , respectively, and the corresponding sideslip angles. The relationship between the tire lateral force and sideslip angle is

$$\begin{cases} F_{y_f}(t) = 2C_f \alpha_f(t) \\ F_{y_r}(t) = 2C_r \alpha_r(t) \end{cases}$$

where α_f and α_r are the slip angles of front and rear tire and can be given by:

$$\begin{cases} \alpha_f(t) = \delta(t) - \frac{l_f \gamma(t)}{v_2} - \beta(t) \\ \alpha_r(t) = \frac{l_r \gamma(t)}{v_2} - \beta(t) \end{cases}$$

However, at high lateral acceleration, the tire/road force may not be linearly proportional to the slip angle owing to differences in the road surface characteristics and cannot be simply expressed in terms of a constant cornering stiffness and sideslip angles. Therefore, we adopt an uncertain cornering stiffness, which varies over a range, to model the uncertainty in the tire/road force^[31]:

$$\begin{cases} F_{y_f}(t) = 2C_f + 2\Delta C_f(\bullet), \\ F_{y_r}(t) = 2C_r + 2\Delta C_r(\bullet). \end{cases} \quad (7)$$

where $C_i = \frac{\max(C_i(\bullet)) + \min(C_i(\bullet))}{2}$, $\Delta C_i(\bullet) \in [-\Delta C_i, \Delta C_i]$, $\Delta C_i = \frac{\max(C_i(\bullet)) - \min(C_i(\bullet))}{2}$ ($i = f, r$), $C_i(\bullet)$ denotes the uncertain cornering stiffness, and (\bullet) represents all possible variables causing variations in the cornering stiffness.

2.4. Vehicle-following system with lateral stability

Longitudinal kinematics, lateral dynamics, and an uncertain tire/road force model are integrated to formulate the following model for closed-loop car-following dynamics [32]:

$$\dot{x}(t) = (\tilde{A} + \Delta\tilde{A})x(t) + \tilde{B}_u u(t) + (\tilde{B}_d + \Delta\tilde{B}_d)d(t), \tag{8}$$

$$\tilde{A} = \begin{bmatrix} 0 & 1 & -t_0 & 0 & 0 \\ 0 & 0 & -1 & 0 & 0 \\ 0 & 0 & -\frac{1}{\tau_0} & 0 & 0 \\ 0 & 0 & 0 & -\frac{2C_f+2C_r}{mv_2} & \frac{2l_r C_r - 2l_f C_f}{mv_2} - 1 \\ 0 & 0 & 0 & -\frac{2l_f C_f - 2l_r C_r}{I_z} & -\frac{2l_f^2 \dot{C}_f + 2l_r^2 \dot{C}_r}{I_z v_2} \end{bmatrix}$$

$$\tilde{B}_u = \begin{bmatrix} 0 & 0 \\ 0 & 0 \\ \frac{1}{\tau_0} & 0 \\ 0 & 0 \\ 0 & \frac{1}{I_z} \end{bmatrix}, \tilde{B}_d = \begin{bmatrix} 0 & 0 \\ 1 & 0 \\ 0 & 0 \\ 0 & \frac{2C_f}{mv_2} \\ 0 & \frac{2l_f \dot{C}_f}{I_z} \end{bmatrix},$$

where $x(t) = [\Delta d, \Delta v, a_2, \beta, \gamma]^T$, $u(t) = [a_{des}, M_z]^T$, and the external disturbance $d(t) = [a_1, \delta]^T$.

The uncertain terms $\Delta\tilde{A}$ and $\Delta\tilde{B}_d$ are denoted as $\Delta\tilde{A} = \tilde{H}_1 F(t) \tilde{E}_1$ and $\Delta\tilde{B}_d = \tilde{H}_1 F(t) \tilde{E}_2$, respectively, where

$$\tilde{H}_1 = \begin{bmatrix} 0 & 0 \\ 0 & 0 \\ 0 & 0 \\ \frac{2\Delta C_f}{mv_2} & \frac{2\Delta C_r}{mv_2} \\ \frac{2l_f \Delta \dot{C}_f}{I_z} & \frac{-2l_r \Delta \dot{C}_r}{I_z} \end{bmatrix}, \tilde{E}_1 = \begin{bmatrix} 0 & 0 \\ 0 & 0 \\ 0 & 0 \\ -1 & -1 \\ \frac{-l_f}{v_x} & \frac{l_r}{v_x} \end{bmatrix}^T,$$

$$F(t) = \begin{bmatrix} N(t) & 0 \\ 0 & N(t) \end{bmatrix}, \tilde{E}_2 = \begin{bmatrix} 0 & 1 \\ 0 & 0 \end{bmatrix},$$

and $N(t) : \mathcal{R}_{t \geq 0} \rightarrow [-1, 1]$ represents an unknown real-value function.

Note that in the car-following scenario, the velocity of the ego vehicle varies with that of the preceding vehicle to maintain a desired safe distance. In this study, we assume that the velocity of the preceding car varies within a bounded range $v_1 \in [v_{min}, v_{max}]$, where v_{min} and v_{max} represent the minimum and maximum velocities during vehicle adaptive cruising.

2.5. T-S fuzzy modeling for longitudinal car-following with vehicle lateral stability

For real-time implementation of the proposed T-S fuzzy model predictive controller in the discrete-time domain, we adopt Euler’s discretization method with the sampling time T_s ; then, the discrete-time model of System Equation (8) is given as

$$x(k + 1) = (A + \Delta A)x(k) + B_u u(k) + (B_d + \Delta B_d)d(k), \tag{9}$$

where

$$A = I + T_s \tilde{A}, \Delta A = I + T_s \Delta \tilde{A},$$

$$B_u = T_s \tilde{B}_u, B_d = T_s \tilde{B}_d, \Delta B_d = T_s \Delta \tilde{B}_d.$$

As the velocity of the ego vehicle v_2 changes with the speed of the preceding vehicle v_1 , Equation (9) is clearly a parameter-varying system.

The T-S fuzzy modelling approach is then employed to describe the time-varying car-following dynamics. We use the classical sector nonlinearity method to derive the discrete-time T-S fuzzy model given in Equation (9):

Fuzzy rule \mathcal{R}^i : if $\theta_1(k) \in \mathcal{F}_1^i$ and $\theta_2(k) \in \mathcal{F}_2^i$, then

$$x(k + 1) = (A_i + \Delta A_i)x(k) + B_u u(k) + (B_{di} + \Delta B_{di})d(k), \tag{10}$$

where $i = 1, 2, \dots, r$, $\theta_1(k) = \frac{1}{v_2}$ and $\theta_2(k) = \frac{1}{v_2}$ are premise variables, \mathcal{F}_j^i is the fuzzy set, and $A_i, B_{di}, \Delta A_i$ and ΔB_{di} are the system matrices defined in Equation (9), with v_2 being replaced by v_{\min} and v_{\max} . We use $\eta(\theta(k))$ to denote the normalized membership function of \mathcal{F}^i , where $\theta(k) = [\theta_1(k), \theta_2(k)]$ represents the premise variable vector, $\mathcal{F}^i = \mathcal{F}_1^i \mathcal{F}_2^i$ and $\sum_{i=1}^r \eta_i(\theta(k)) = 1$. For brevity, $\eta_i(\theta(k))$ is denoted as η_i . Considering the velocity restrictions enables us to easily derive the following weighting factors for the established T-S fuzzy system [Equation (10)]:

$$\mathcal{F}_{1\max} = \frac{\theta_{1\max} - \theta_1}{\theta_{1\max} - \theta_{1\min}}, \quad \mathcal{F}_{1\min} = \frac{\theta_1 - \theta_{1\min}}{\theta_{1\max} - \theta_{1\min}}, \tag{11}$$

$$\mathcal{F}_{2\max} = \frac{\theta_{2\max} - \theta_2}{\theta_{2\max} - \theta_{2\min}}, \quad \mathcal{F}_{2\min} = \frac{\theta_2 - \theta_{2\min}}{\theta_{2\max} - \theta_{2\min}}, \tag{12}$$

where $\theta_{1\max}, \theta_{2\max}, \theta_{1\min}$ and $\theta_{2\min}$ are the maximal and minimal values of θ_1 and θ_2 , respectively, and $\mathcal{F}_j^i (i = 1, 2, 3, 4, j = 1, 2)$ can be obtained accordingly from Equation (11) and Equation (12). Therefore, \mathcal{F}^i is derived from 2^2 combinations of \mathcal{F}_1^i and \mathcal{F}_2^i . The following compact representation of Equation (9) is obtained by using a standard fuzzy inference approach:

$$x(k + 1) = \mathcal{A}(\eta)x(k) + \mathcal{B}_u u(k) + \mathcal{B}_d(\eta)d(k), \tag{13}$$

where

$$\begin{cases} \mathcal{A}(\eta) = A(\eta) + \Delta A(\eta) = \sum_{i=1}^r \eta_i (A_i + \Delta A_i) \\ \mathcal{B}_u(\eta) = \sum_{i=1}^r \eta_i B_{ui} \\ \mathcal{B}_d(\eta) = B_d(\eta) + \Delta B_d(\eta) = \sum_{i=1}^r \eta_i (B_{di} + \Delta B_{di}) \\ \eta = \eta(k) = [\eta_1, \dots, \eta_r]. \end{cases}$$

Note that using the sector nonlinearity modelling approach with the premise variables $\frac{1}{v_2}$ and $\frac{1}{v_2}$ yields a T-S fuzzy expression for the car-following system with lateral stability. The discretized form of the tracking system in Equation (9) is represented using $r = 2^2$ linear subsystems with the aforementioned membership functions. Inspired by [33], we further exploit the relationships among the premise variables to reduce the numerical computational complexity and conservativeness of the controller design. Here, we define

$$v_2 = \frac{\hat{v}_0 \hat{v}_1}{\hat{v}_1 + \hat{v}_0 \rho}, \tag{14}$$

where ρ is a scalar variable, $\hat{v}_0 = \frac{2v_{\min}v_{\max}}{v_{\min}+v_{\max}}$ and $\hat{v}_1 = \frac{2v_{\min}v_{\max}}{v_{\min}-v_{\max}}$. Therefore, we have

$$\frac{1}{v_2} = \frac{1}{\hat{v}_0} + \frac{1}{\hat{v}_1} \rho. \tag{15}$$

The new premise variable ρ is bounded as follows:

$$\rho \in [-1, 1], \tag{16}$$

where $v_2 = v_{\min}$ for $\rho = -1$ and $v_2 = v_{\max}$ for $\rho = 1$. Therefore, ρ can be used to describe the variation in v_2 from v_{\min} to v_{\max} . In addition, the following equation can be obtained based on Taylor's approximation:

$$\frac{1}{v_2} \simeq \frac{1}{\hat{v}_0} (1 + 2 \frac{\hat{v}_0}{\hat{v}_1} \rho). \tag{17}$$

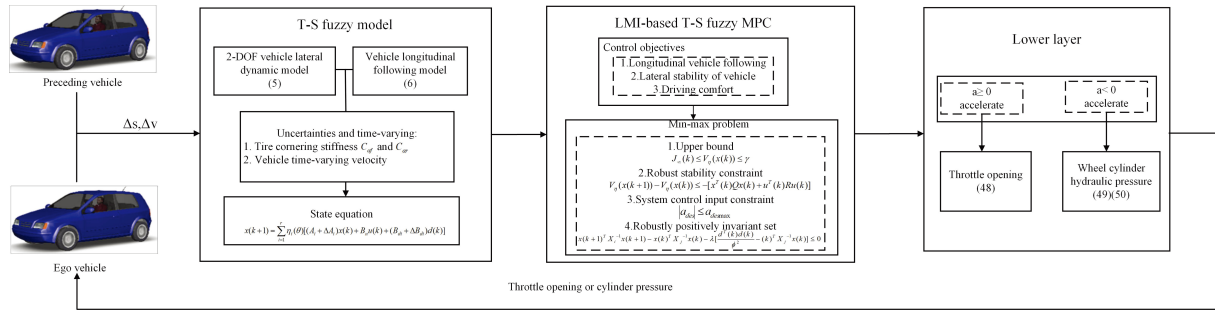


Figure 3. The whole algorithm framework.

The number of subsystems in the T-S fuzzy model Equation (10) is thus reduced from 4 to 2, which considerably decreases the computational burden associated with the controller parameters in each sampling period within the MPC framework, and facilitates real-time implementation of the model, as expected.

3. T-S FUZZY MODEL PREDICATIVE CONTROL DESIGN

In this section, we provide a detailed description of the design of an adaptive cruise controller with lateral stability based on the T-S fuzzy MPC framework. Figure 3 shows the proposed adaptive cruise control system divided into upper and lower layers. The upper layer calculates the required acceleration and direct yaw moment for vehicle-following control subject to various constraints, and the lower layer calculates the vehicle throttle opening or hydraulic cylinder pressure of the four wheels to generate control signals corresponding to the results provided by the upper layer. Before proceeding further, some definitions and lemmas are first stated.

3.1. Robust positively invariant set

Consider a discrete-time dynamical system

$$x(k + 1) = f(x(k), d(k)), \tag{18}$$

where $f(0, 0) = 0$, $x(k) \in \mathbb{R}^n$ is a state vector, and $d(k)$ is a control input or external disturbance that belongs to a compact set $\mathbb{D} \subset \mathbb{R}^m$ containing the origin. A robust positively invariant (RPI) set is defined below.

Definition 3.1: If $x(k) \in \Omega$ ($\Omega \subset \mathbb{R}^n$), it holds that $x(k + 1) \in \Omega$ for all $d(k) \in \mathbb{D}$; then, Ω is called an RPI set for System [Equation (18)].

Lemma 3.1 [34]: The following two expressions are equivalent for System [Equation (18)] with $d^T d \leq c^2$, where c is a positive constant:

- the ellipsoidal set $\Omega_p \triangleq \{x^T P x \leq \gamma\}$, where $P > 0$, is a robust positively invariant set;
- the inequality $x(k + 1)^T P x(k + 1) \leq x^T P x$ holds if the external disturbance satisfies $\frac{1}{c^2} d^T d \leq \frac{1}{\gamma} x^T P x$.

3.2. Input-to-state stability

We define input-to-state stability (ISS) for use in the following sections.

Definition 3.2: A discrete-time system $x(k + 1) = f(x(k), d(k))$ is ISS if there exist a \mathcal{KL} -function $\beta : \mathbb{R}_{\geq 0} \times \mathbb{Z}_+ \rightarrow \mathbb{R}_{\geq 0}$ and a \mathcal{K} -function ρ satisfying

$$\|x(k, x_0, d(k))\| \leq \beta(\|x_0\|, k) + \rho(\sup_{k \geq 0} \|d(k)\|), \tag{19}$$

where x_0 is the initial state, $d(k)$ is the input sequence, and k is the sampling time instant.

Definition 3.3: A function $V : \mathbb{R}^n \rightarrow \mathbb{R}_{\geq 0}$ is called an ISS-Lyapunov function for the system $x(k + 1) = f(x(k), d(k))$ if there exist \mathcal{K}_∞ -functions $\alpha_1, \alpha_2, \alpha_3$ and a \mathcal{K} -function ρ satisfying

$$\begin{aligned} \alpha_1(\|x(k)\|) &\leq V(x(k)) \leq \alpha_2(\|x(k)\|), \\ V(x(k + 1)) - V(x(k)) &\leq -\alpha_3(\|x(k)\|) + \rho(\sup_{k \geq 0} \|d(k)\|). \end{aligned}$$

Lemma 3.2^[35]: A system is said to have ISS if it admits a continuous ISS-Lyapunov function.

3.3. T-S fuzzy model-based predictive control

We adopt the following model within the framework of predictive control to represent the future dynamics of the T-S fuzzy system for vehicle-following considering lateral stability:

$$x(k + i + 1|k) = \mathcal{A}(\eta)x(k + i|k) + \mathcal{B}_u u(k + i|k) + \mathcal{B}_d(\eta)d(k + i|k), \tag{20}$$

where $x(k + i|k)$, $u(k + i|k)$ and $d(k + i|k)$ represent the predicted state, control input and external disturbances at the $(k + i)$ th time instant, respectively, and $i \in \{1, 2, \dots\}$. The stage cost $\ell(k + i|k)$ can be represented as

$$\ell(k + i|k) = x(k + i|k)^T Q x(k + i|k) + u(k + i|k)^T R u(k + i|k) - \tau d(k + i|k)^T d(k + i|k) \tag{21}$$

where Q and R are the weighting matrices of the state variables of the system and control inputs, respectively. τ is the weight related to the external disturbance. We simplify this notation by using $x(k + i)$, $u(k + i)$ and $d(k + i)$ to denote $x(k + i|k)$, $u(k + i|k)$ and $d(k + i|k)$, respectively.

Consider the following objective function \mathcal{J}_p

$$\mathcal{J}_p(k) = \sum_{i=0}^{p-1} \ell(k + i|k) + V(x(k + p|k)), \tag{22}$$

where $\ell(k + i|k)$ is the stage cost at the predicated time instant, and the positive-definite function $V(x(k + p|k))$ is called the terminal cost. This type of cost function was proposed in Ref.^[36] to develop a novel synthesis method with enhanced robustness.

As the cost function cannot be optimized in real time due to the unknown external disturbance, the upper limit of the cost function is minimized here. We define the following fuzzy quadratic Lyapunov function:

$$V(x(k)) = \sum_{i=1}^2 \eta_i(\theta)x(k)^T P_i x(k) = x(k)^T P(\eta)x(k) \tag{23}$$

where P_j is a positive definite matrix. Let the Lyapunov function satisfy the following inequality constraint:

$$V(x(k + i + 1)) - V(x(k + i)) \leq [x(k + i)^T Q x(k + i) + u(k + i)^T R u(k + i) - \tau d(k + i)^T d(k + i)]. \tag{24}$$

Add both sides of the inequality from $i = 0$ to ∞ , then we get

$$\mathcal{J}_\infty(k) \leq V(x(k)) - V(x(\infty)),$$

which implies that we can infer the upper bound of the objective function \mathcal{J}_∞ from the positiveness property of the function $V(x(\infty))$. Assume a scalar γ exists that satisfies

$$V(x(k)) \leq \gamma. \tag{25}$$

Defining $X_j = \gamma P_j^{-1}$ and applying the Schur complement operation yields the following sufficient condition for Equation (24):

$$\begin{bmatrix} 1 & x(k)^T \\ x(k) & X_j \end{bmatrix} \geq 0. \tag{26}$$

Then, the aforementioned optimization problem is converted into the minimization of the upper bound of the infinite-horizon objective function:

$$\begin{aligned} & \min \gamma \\ & \text{s.t. Equation (25)}. \end{aligned} \tag{27}$$

A state feedback law $u(k) = F_\eta x(k)$ is applied to minimize the upper bound of the performance functions \mathcal{J}_p and $F_\eta = \sum_{j=1}^n \eta_j(\theta) F_j$, where $F_j = Y_j X_j$. Considering the inequality [Equation (24)] yields

$$\begin{aligned} & x(k)^T \left[(A(\eta) + \Delta A(\eta) + B_u(\eta) F_\eta)^T P_\eta * -P_\eta + Q + F_\eta^T R F_\eta \right] x(k) \\ & + x(k)^T (A(\eta) + \Delta A(\eta) + B_u(\eta) F_\eta)^T P_\eta (B_d(\eta) + \Delta B_d(\eta)) * d(k) \\ & + d(k)^T (B_d(\eta) + \Delta B_d(\eta))^T P_\eta (A(\eta) + \Delta A(\eta) + B_u(\eta) F_\eta) x(k) \\ & + d(k)^T [(B_d(\eta) + \Delta B_d(\eta))^T P_\eta * -\tau I] d(k) \leq 0, \end{aligned} \tag{28}$$

which is equivalent to

$$\begin{bmatrix} x(k) \\ d(k) \end{bmatrix}^T \begin{bmatrix} \Pi_1 & \Pi_2 \\ * & \Pi_3 \end{bmatrix} \begin{bmatrix} x(k) \\ d(k) \end{bmatrix} \leq 0, \tag{29}$$

$$\begin{aligned} \Pi_1 &= [A(\eta) + \Delta A(\eta) + B_u(\eta) Y_\eta]^T P_\eta * -P_\eta + Q + F_\eta^T R F_\eta \\ \Pi_2 &= [A(\eta) + \Delta A(\eta) + B_u(\eta) F_\eta]^T P_\eta [B_d(\eta) + \Delta B_d(\eta)] \\ \Pi_3 &= [B_d(\eta) + \Delta B_d(\eta)]^T P_\eta * -\tau I. \end{aligned} \tag{30}$$

I is an identity matrix with appropriate dimensions. The inequality [Equation (28)] can be guaranteed as long as

$$\begin{bmatrix} \Pi_1 & \Pi_2 \\ * & \Pi_3 \end{bmatrix} \leq 0 \tag{31}$$

holds.

Here, we introduce a lemma for use in the following sections.

Lemma 3.3 [37]: For matrices Γ , H and E with appropriate dimensions and $\Gamma^T = \Gamma$, the following inequality

$$\Gamma + HF(k)E + E^T F(k)H^T \leq 0 \tag{32}$$

holds for all $F(k)^T F(k) \leq 1$ if and only if there is a positive scalar ϵ such that

$$\Gamma + \epsilon E^T E + \frac{1}{\epsilon} H H^T \leq 0. \tag{33}$$

By *Lemma 3.3*, the following sufficient condition can be derived to guarantee the inequality [Equation (31)]:

$$\begin{bmatrix} -X_i & 0 & (A_j X_j + B_{uj} Y_j)^T & (Q X_j)^T & (R Y_j)^T & (E_{j1} X_j)^T & 0 \\ * & -\zeta I & \gamma B_{dj}^T & 0 & 0 & 0 & (\gamma E_{j2})^T \\ * & * & \epsilon_j (H_{j1} H_{j1}^T + H_{j2} H_{j2}^T) - X_j & 0 & 0 & 0 & 0 \\ * & * & * & -\gamma Q & 0 & 0 & 0 \\ * & * & * & * & -\gamma R & 0 & 0 \\ * & * & * & * & * & -\epsilon_j I & 0 \\ * & * & * & * & * & * & -\epsilon_j I \end{bmatrix} \leq 0, j = 1, 2, \tag{34}$$

where $\zeta = \gamma \tau$.

We also need to consider the control input constraints to ensure driving comfort:

$$|u_i(k)| \leq u_{i,\max}, \quad i = 1, 2 \tag{35}$$

According to inequality [Equation (26)], we have:

$$x(k)^T X_j^{-1} x(k) \leq 1. \tag{36}$$

Therefore, we have:

$$\begin{aligned} \max \|u(k)\|^2 &= \max \|(F(\eta)x(k))\|^2 \\ &= \max \|(Y(\eta)X(\eta)^{-1}x(k))\|^2 \\ &= \max \|(Y(\eta)X(\eta)^{-\frac{1}{2}}X(\eta)^{-\frac{1}{2}}x(k))\|^2 \\ &\leq \|(Y(\eta)X(\eta)^{-\frac{1}{2}})\|^2 \|X(\eta)^{-\frac{1}{2}}x(k)\|^2 \\ &= (Y(\eta)X(\eta)^{-1}Y(\eta))[x(k)^T X(\eta)^{-1}x(k)] \\ &\leq Y(\eta)X(\eta)^{-1}Y(\eta). \end{aligned} \tag{37}$$

Considering the Schur complement, the input constraint can be guaranteed by the following LMI if there exists a symmetric matrix U [38]

$$\begin{bmatrix} U & Y_j \\ * & X_j \end{bmatrix} \geq 0, \tag{38}$$

where $U_{ii} \leq u_{i,\max}^2$.

To deal with the external disturbance, the concept of RPI is introduced to ensure the closed-loop stability of car-following system. According to the concept of RPI and quadratic boundedness as shown in Lemma 3.1, Ω_k is an RPI set if

$$x(k+1|k)^T P_i x(k+1|k) \leq x(k|k)^T P_j x(k|k)$$

holds under

$$\frac{d(k)^T d(k)}{\phi^2} \leq x(k)^T Q_j^{-1} x(k),$$

where $d(k)^T d(k) \leq \phi^2$.

The S-procedure is used to obtain a sufficient condition as follows:

$$x(k+1)^T X_i^{-1} x(k+1) - x(k)^T X_j^{-1} x(k) - \lambda \left[\frac{d(k)^T d(k)}{\phi^2} - x(k)^T X_j^{-1} x(k) \right] \leq 0, \tag{39}$$

where λ is a positive scalar belonging to (0, 1).

By Lemma 3.3, the above mentioned inequality can be guaranteed by the following matrix: inequality:

$$\begin{bmatrix} (-1 + \lambda)X_i & 0 & (A_j X_j + B_{uj} Y_j)^T & (E_{j1} X)^T & 0 \\ * & -\frac{\lambda}{\phi^2} I & (B_{dj})^T & 0 & (E_{j2})^T \\ * & * & \epsilon_j (H_{j1} H_{j1}^T + H_{j2} H_{j2}^T) - X_j & 0 & 0 \\ * & * & * & -\epsilon_j I & 0 \\ * & * & * & * & -\epsilon_j I \end{bmatrix} \leq 0, \quad j = 1, 2. \tag{40}$$

Therefore, the controller design can be summarized as the following:

$$\begin{aligned} & \min_{x_j > 0, \epsilon_j > 0, Y_j} \zeta \\ \text{s. t. } & (26), (34), (38), (40), \text{ and } 0 < \lambda < 1. \end{aligned} \quad (41)$$

The T-S fuzzy state feedback controller is derived by solving the optimization problem in Equation (40) under parameter uncertainties and external persistent perturbations. The inequality Equation (34) ensures that the cost function $\mathcal{J}_\infty(k)$ is upper-bounded by the Lyapunov function $V(x(k))$, the inequality Equation (38) guarantees that the input constraints are satisfied, and the inequality Equation (40) leads to $x(k) \in \Omega_k$, where Ω_k is an RPI set.

Remark 3.1: Note that ζ is minimized instead of γ in the abovementioned optimization problem. This approach is used because both γ and τ need to be minimized, and a smaller τ implies a higher system performance. We adopt the approach given in Ref. [23] to simultaneously optimize γ and τ by defining $\zeta = \gamma\tau$ in Equation (34). The introduction of the variable λ makes the constraint Equation (40) a bilinear matrix inequality, which can be handled with existing solvers, e.g., PENBMI. The computational load is reduced further by predefining a suboptimal value of λ by trial and error.

Theorem 3.1: The optimization problem Equation (40) has the property of recursive feasibility, that is, a solution will always exist once the problem is initially solvable.

Proof: Implementation of the predictive control strategy based on the T-S fuzzy model requires the constrained optimization problem Equation (40) to be solved at each time instant. Therefore, it is important to guarantee the recursive feasibility of the optimization problem. As an external disturbance is considered, the recursive feasibility is no longer a natural characteristic of the proposed controller. In this study, only the constraint Equation (26) depends on the time instant k , which involves $x(k)$. Therefore, we only need to ensure the feasibility of the constraint Equation (26).

Note that the inequality Equation (26) is equal to $x(k) \in \Omega_k$. The inequality Equation (40) ensures that the set Ω_k is an RPI set, which implies that the inequality Equation (26) is still feasible at the $(k + 1)$ time instant. That is, $x(k + 1) \in \Omega_{k+1} \in \Omega_k$ is still satisfied. Hence, recursive feasibility is guaranteed. Thus, the proof is completed. \square

Theorem 3.2: The closed-loop system in this paper has ISS based on the proposed MPC strategy under an external disturbance.

Proof: It has been proven that the optimization problem Equation (41), once solvable, will always be solvable.

Define the optimal solution at time instant k as $\{\gamma^*, X_j^*, \epsilon_{1j}^*, \epsilon_{2j}^*, Y_j^*, \zeta^*\}$, and $V^*(x(k)) = \sum_{i=1}^2 \eta_i(\theta) x^T(k) P_i^* x(k)$, where $P^* = \gamma^* X_j^{*-1}$. We need to prove that the $V^*(x(k))$ is an ISS-Lyapunov function. Define $\bar{\lambda}$ as the upper bound of eigenvalue of P_η^* , and $\underline{\lambda}$ as the lower bound of the eigenvalue of P_η^* . We can obtain:

$$\underline{\lambda} \|x(k)\|^2 \leq V^*(x(k)) \leq \bar{\lambda} \|x(k)\|^2. \quad (42)$$

Furthermore, from inequality Equation (24), we can derive the following inequality:

$$V^*(x(k+1)) - V^*(x(k)) \leq -x(k)^T Q x(k) - x(k)^T F^{*T} R F^* x(k) + \tau d(k)^T d(k), \quad (43)$$

where $F^* = \sum_{j=1}^2 \eta_j(\theta) Y_j X_j^{-1}$. Therefore, we get

$$V^*(x(k+1)) - V^*(x(k)) \leq -x(k)^T Q x(k) + \tau d(k)^T d(k). \quad (44)$$

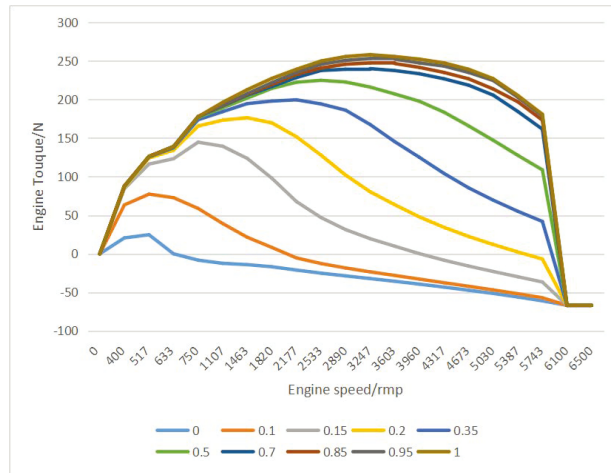


Figure 4. Engine model.

From the inequalities Equation (42), Equation (44) and Lemma 3.2, we can conclude that $V(x(k))$ is an ISS-Lyapunov function, and the closed-loop system is ISS. Thus the proof is completed. \square

4. LOWER LAYER

According to the vehicle longitudinal motions in the car-following scenario, the lower layer is divided into two blocks for calculating the acceleration throttle opening and the brake pressure, which are designed to realize the desired longitudinal acceleration or deceleration and direct yaw moment. To this end, a logic switch in the lower layer is utilized to implement an accelerating or braking manoeuvre based on the desired longitudinal acceleration a_{des} and the direct yaw moment M_{des} calculated by the T-S fuzzy controller in the upper layer. The vehicle throttle opening or brake pressure on all four wheels can then be obtained.

4.1. Accelerating control

Figure 4 shows the engine speed versus the torque at different throttle openings, which are shown at the bottom. If the engine speed w_e and the desired torque $T_{e,des}$ are known, the corresponding expected throttle opening σ_{des} is obtained based on this look-up table:

$$\sigma_{des} = f(T_{e,des}, w_e). \tag{45}$$

The vehicle longitudinal dynamics are produced by the combined effect of vehicle traction, wind resistance, and ground resistance. Therefore, the vehicle state depends strongly on the road smoothness and the magnitude of the wind resistance coefficient during cruising. The equivalent air friction during longitudinal driving is

$$F_f = \frac{1}{2} \rho_a C_d A_F (r_{eff} R_p w_e)^2, \tag{46}$$

where ρ_a is the air mass density, C_d is the coefficient of air friction, A_F is the windward area of the ego vehicle, R_p is the ratio between the wheel speed w_w and engine speed w_e , and r_{eff} is the effective tire radius.

During vehicle acceleration, the engine torque $T_{e,des}$ is related to the expected acceleration a_{des} is [39] as

$$T_{e,des} = \frac{J_e}{R_p r_{eff}} a_{des} + [c_a R_p^3 r_{eff}^3 w_e^2 + R_p (r_{eff} R_x)], \tag{47}$$

where $J_e = I_e + I_t + (mr_{eff}^2 + I_w)R_p^2$ is the effective moment of inertia for the engine side, I_e is the moment of inertia of the engine, and R_x is the sum of all the rolling resistances related to the rolling damping coefficient

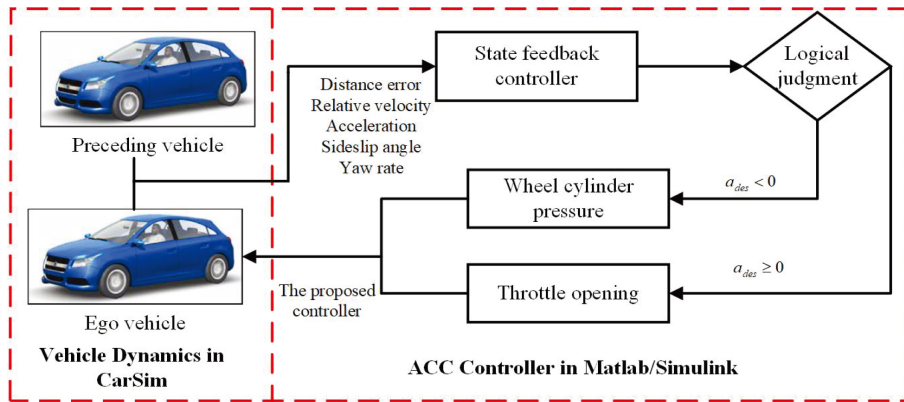


Figure 5. Structure of the car-following systems in Carsim/Simulink joint simulation environment.

f. As $f \in (0.01, 0.04)$, R_x is sufficiently small to be neglected in this study. The following exist:

$$m \gg \frac{I_e}{r_{\text{eff}}^2}, \quad m \gg \frac{I_t}{r_{\text{eff}}^2}, \quad m \gg \frac{I_w}{r_{\text{eff}}^2}. \tag{48}$$

Then, J_e can be rewritten as $J_e = mr_{\text{eff}}^2 R_p^2$. Therefore, Equation (47) can be rewritten as follows:

$$T_{e,\text{des}} = R_p r_{\text{eff}} (m a_{\text{des}} + F_f). \tag{49}$$

Thus, the corresponding expected throttle opening σ_{des} can be obtained from the inverse dynamic relation.

4.2. Braking control

During vehicle braking, the desired acceleration a_{des} and the yaw moment M_{des} given by the upper controller can be used to determine the longitudinal tire force from the following equation [40]:

$$\begin{cases} -m a_{\text{des}} = F_{fl} + F_{fr} + F_{rl} + F_{rr} \\ M_{\text{des}} = (F_{fr} + F_{rr} - F_{fl} - F_{rr}) b \\ F_{rl} = \frac{l_f g + a_2 h}{l_r g - a_2 h} F_{fl} \\ F_{rr} = \frac{l_f g + a_2 h}{l_r g - a_2 h} F_{fr} \end{cases}, \tag{50}$$

where b is the distance between the right and left wheels and h is the height of the centre of mass of the vehicle.

Equation (50) can be solved for the longitudinal force on the four wheels. Then, we can calculate the hydraulic pressure wheel cylinder from the following equation:

$$P_{B,ij} = \frac{r_w}{K_B} F_{ij}, \tag{51}$$

where r_w denotes the efficient wheel radius and K_B represents the pressure constant of a single wheel.

5. SIMULATION VALIDATIONS

CarSim/Simulink joint simulations are conducted to verify the effectiveness of the proposed predictive control based on the T-S fuzzy model. The structure of the car-following system is shown in Figure 5. The proposed controller is derived by solving the optimization problem in Equation (41) with the YALMIP toolbox introduced in [41] within the MATLAB/Simulink environment, where the vehicle model and road conditions are provided by the CarSim platform. We simulate a severe riding condition by considering a road with snow cover on the left-hand side of the vehicle. The test scenario is shown in Figure 6.

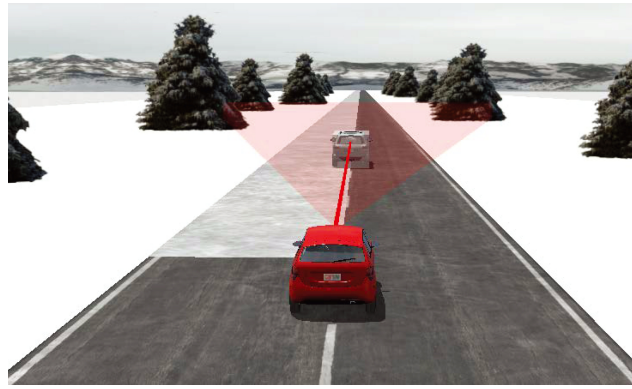


Figure 6. The scenario setting in Carsim platform.

Table 1. Parameters in the simulation model

Parameters	Values
m (kg)	1110
I_z (kg/m ²)	1343.1
τ_0 (s)	0.25
b (mm)	1480
h (mm)	350
r_{eff} (mm)	298
t_0 (s)	2
$C_{\alpha f}$ (N/rad)	66900
$C_{\alpha r}$ (N/rad)	62700

The B-Class Hatchback car is selected as the ego vehicle to be controlled, and its physical parameters are given in [Table 1](#). We illustrate the advantages of the methods developed in this study by comparison against a conventional controller design without vehicle lateral stabilization.

The preceding vehicle is set to be 60m ahead of the ego vehicle at the start of the simulation. We compare the simulation results for two different speed profiles: (1) a ramp speed profile and (2) a *cosine* speed profile.

5.1. Case I: ramp speed profile

The initial condition in this case is a zero relative velocity between vehicles: we assume $v_1 = v_2 = 25$ m/s and a desired distance between vehicles at standstill $d_0 = 10$ m. Considering the nonlinearity of the lateral forces between the tires and the road surface, the cornering stiffness for the front and rear tires is set to (66900 ± 10000) N/rad and (62700 ± 10000) N/rad, respectively. The upper bound on the control input for the vehicle acceleration is set to 2 m²/s. Substituting the corresponding parameters into the system model [Equations 8-17](#) easily yields the system matrices. According to [Remark 3.1](#), λ is selected as 0.01 in this study.

The optimization problem given by [Equation \(41\)](#) is solved recursively to yield the closed-loop system responses in the CarSim/Simulink joint simulation environment, which are shown in [Figure 7](#). In [Figure 7A](#), the blue and red curves represent the speeds of the preceding and ego vehicles, respectively. [Figure 7B](#) and [Figure 7C](#) show the errors in the longitudinal velocity and between the desired and actual longitudinal distances, respectively, where the maximum velocity error is 5.9 m/s at 4.5 s and the maximum distance error is 3.8 m at 19.7 s. [Figure 7](#) shows that although the preceding vehicle velocities vary in the range [10, 25] m/s, the predictive controller based on the T-S fuzzy model guarantees the velocity and the desired safe following distance for the ego vehicle under the considered extreme road conditions.

To further demonstrate the advantages of the proposed car-following controller design, [Figure 8](#) shows the

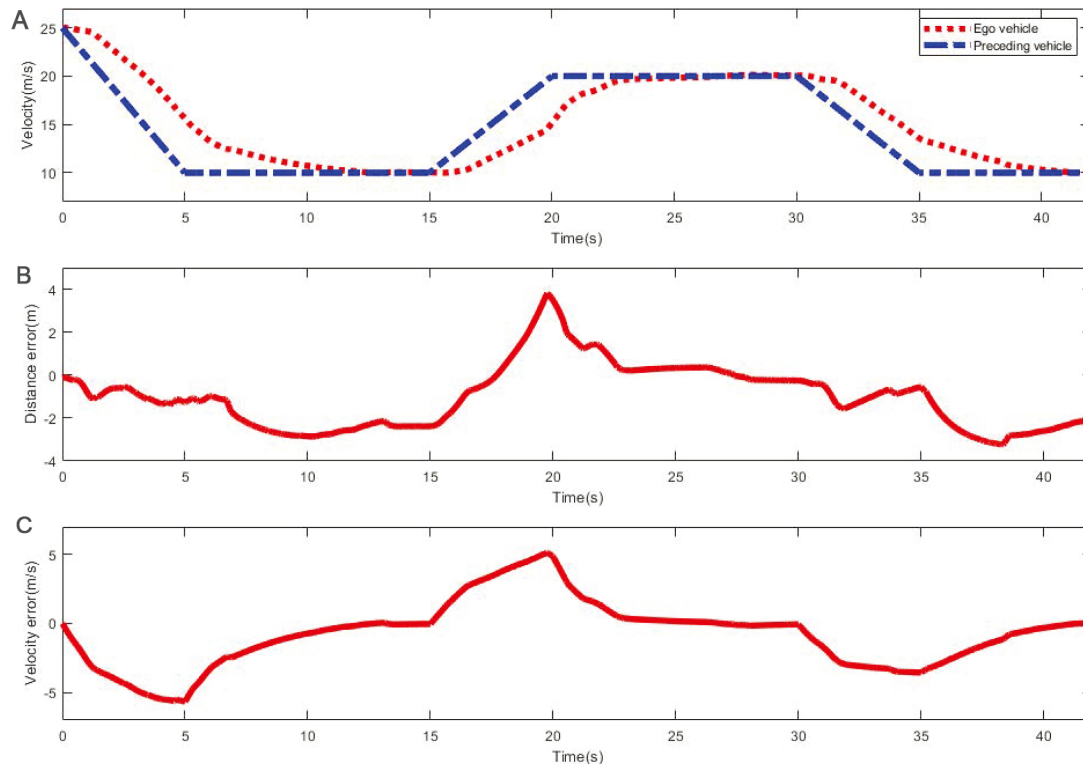


Figure 7. (A) Velocity of the preceding and ego vehicle; (B) Relative velocity; (C) Relative distance.

responses of sideslip angles and yaw rate (which reflect the lateral stability of the vehicle) obtained using the conventional controller (without consideration of the lateral stability) and the controller developed in this study. [Figure 8](#) shows that compared to the results obtained using the conventional controller, the sideslip angle and yaw rate obtained using the proposed controller are smaller in magnitude, indicating improved vehicle stability.

5.2. Case II: *cosine* speed profile

In this case, the initial velocities of the preceding and ego vehicles and the relative distance are set to 25 m/s and 50 m, respectively. [Figure 9A](#) shows the *cosine*-function speed profile of the preceding vehicle and the simulation results as a blue dash-dotted curve. In [Figure 9A](#), the red curve represents the closed-loop response for the speed of the ego vehicle. [Figure 9B](#) and [Figure 9C](#) show the errors in the longitudinal velocity and between the desired and actual distances, respectively. [Figure 9D](#) shows the acceleration of the ego vehicle, which satisfies the input constraint given by $|a_{des}| \leq 2 \text{ m}^2/\text{s}$.

It can be concluded from [Figure 9](#) that the proposed method completes the car-following task with satisfactory performance for a time-varying velocity. [Figure 10](#) shows the dynamics of the sideslip angle, yaw rate, and vehicle lateral offset. [Figure 10C](#) clearly shows that the lateral offset increases when the car-following manoeuvre is conducted under the conventional MPC without lateral stabilization. These three aspects of the results show that the proposed car-following controller outperforms the conventional controller in terms of guaranteeing both satisfactory tracking performance and lateral stability of the vehicle in emergency scenarios.

6. CONCLUSION

In this paper, a T-S fuzzy model-based predictive adaptive cruise controller is designed while ensuring vehicle lateral stability by integrating the ACC system with a direct yaw moment control system. To consider varia-

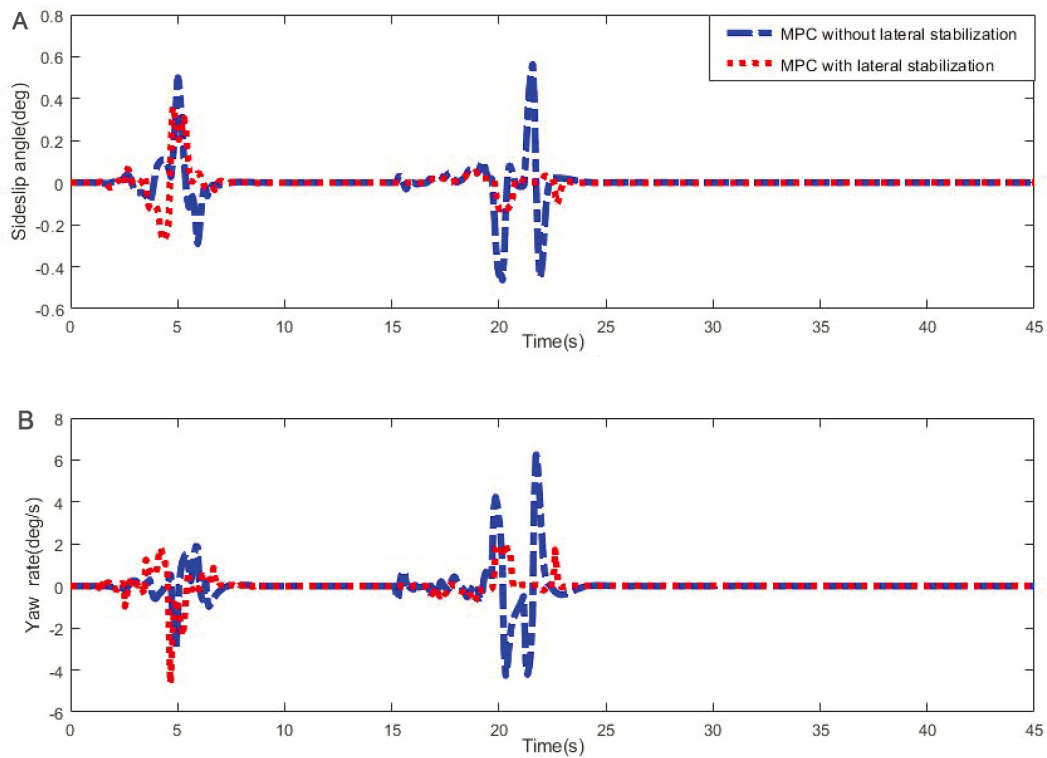


Figure 8. (A) Vehicle sideslip angle of the ego vehicle in Case I. (B) Vehicle yaw rate of the ego vehicle in Case I.

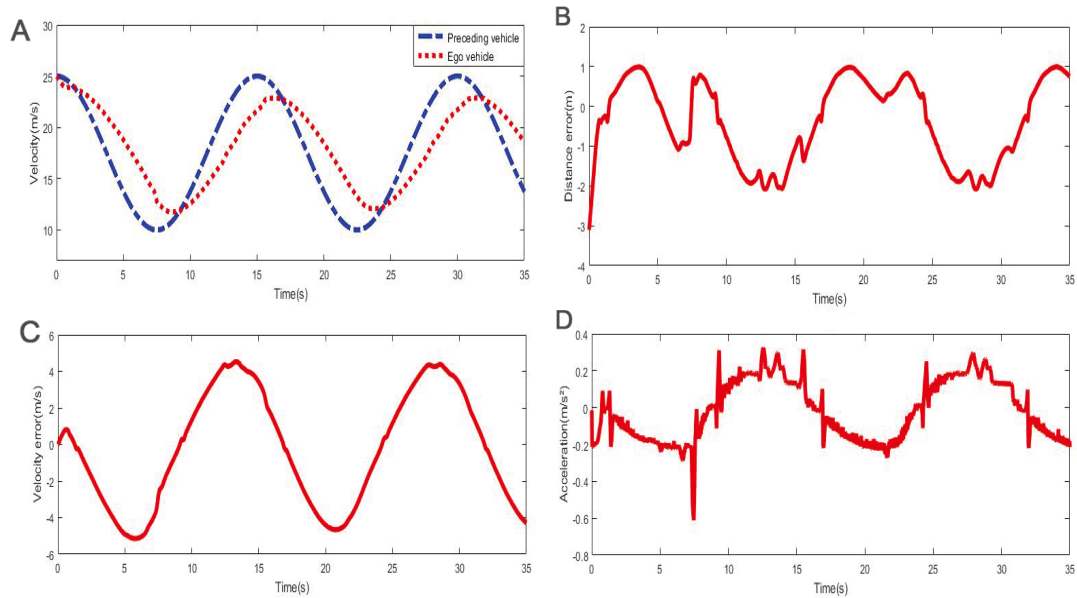


Figure 9. (A) Velocity of preceding and ego vehicle; (B) Relative velocity; (C) Relative distance; (D) Ego vehicle acceleration.

tions in the preceding vehicle velocity and road surface conditions, the adaptive cruise control is formulated as a tracking control problem of a T-S fuzzy system subject to parameter uncertainties and external persistent perturbations. Then, a robust positively invariant set is introduced to develop an admissible T-S fuzzy controller by solving a min-max optimization problem under a series of linear matrix inequality constraints.

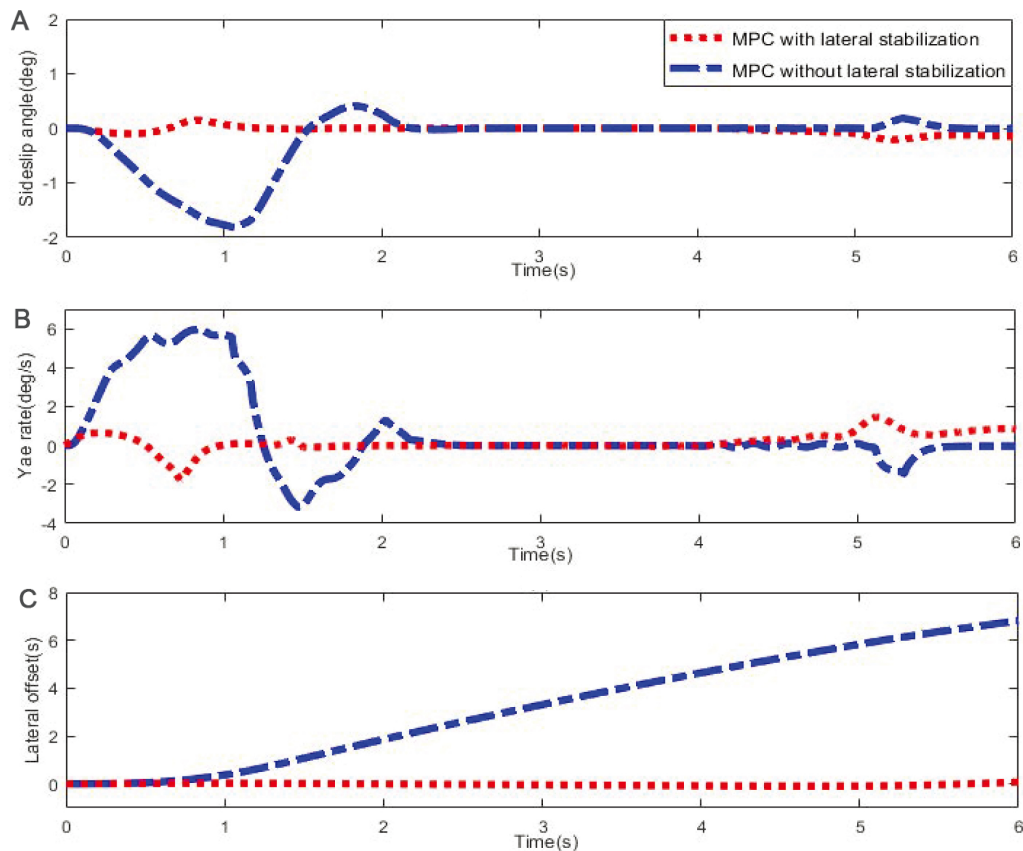


Figure 10. (A) Sideslip angle in Case II; (B) Yaw rate in Case II; (C) Vehicle lateral offset in Case II.

CarSim/Simulink joint simulation results verify that the developed method exhibits good performance for vehicle tracking and ensures vehicle lateral stability.

DECLARATIONS

Authors' contributions

Made substantial contributions to conception and design of the study and performed data analysis and interpretation: Zhang C, Wei X

Performed data acquisition, as well as provided administrative, technical, and material support: Wang Z, Zhang H, Guo X

Availability of data and materials

In this paper, we have detailed a modelling procedure and the construction of an optimization problem with linear matrix inequality constraints to design a T-S fuzzy model predictive controller. The physical parameters of the vehicle are provided in the section on the simulations. The effectiveness of the developed method has been demonstrated using the MATLAB/CarSim joint simulation platform. There are no additional data or materials associated with this study.

Financial support and sponsorship

This work was supported in part by National Key R&D Program of China under Grant No: 2020AAA0108100; in part by Shanghai Natural Science Foundation under Grant No: 21ZR1482300 and 19ZR1461400; and in part by the Fundamental Research Funds for the Central Universities.

Conflicts of interest

All authors declared that there are no conflicts of interest.

Ethical approval and consent to participate

Not applicable.

Consent for publication

Not applicable.

Copyright

© The Author(s) 2022.

REFERENCES

1. Hasenjäger M, Heckmann M, Wersing H. A survey of personalization for advanced driver assistance systems. *IEEE Trans Intell Veh* 2020;5:335–44. [DOI](#)
2. Li L, Wen D, Zheng N, Shen L. Cognitive cars: a new frontier for ADAS research. *IEEE Trans Intell Trans Syst* 2012;13:395–407. [DOI](#)
3. Muresan MP, Nedeveschi S. Multimodal sparse LIDAR object tracking in clutter. In: 2018 IEEE 14th International Conference on Intelligent Computer Communication and Processing (ICCP); 2018. pp. 215–21. [DOI](#)
4. Cheng J, Ju M, Zhou M, Liu C, Gao S, et al. A dynamic evolution method for autonomous vehicle groups in a highway scene. *IEEE Int Things J* 2022;9:1445–57. [DOI](#)
5. Yuan T, Krishnan K, Duraisamy B, Maile M, Schwarz T. Extended object tracking using IMM approach for a real-world vehicle sensor fusion system. In: 2017 IEEE International Conference on Multisensor Fusion and Integration for Intelligent Systems (MFI); 2017. pp. 638–43. [DOI](#)
6. Guo C, Meguro J, Kojima Y, Naito T. A multimodal ADAS system for unmarked urban scenarios based on road context understanding. *IEEE Trans Intell Transp Syst* 2015;16:1690–704. [DOI](#)
7. Hosseinnia SH, Tejado I, Milanés V, Villagrà J, Vinagre BM. Experimental application of hybrid fractional-order adaptive cruise control at low speed. *IEEE Trans Contr Syst Techn* 2014;22:2329–36. [DOI](#)
8. Wang X, Chen M, Zhu M, Tremont P. Development of a kinematic-based forward collision warning algorithm using an advanced driving simulator. *IEEE Trans Intell Trans Syst* 2016;17:2583–91. [DOI](#)
9. Pananurak W, Thanok S, Parnichkun M. Adaptive cruise control for an intelligent vehicle. In: 2008 IEEE International Conference on Robotics and Biomimetics; 2009. pp. 1794–99. [DOI](#)
10. Asadi B, Vahidi A. Predictive cruise control: utilizing upcoming traffic signal information for improving fuel economy and reducing trip time. *IEEE Trans Contr Syst Techn* 2011;19:707–14. [DOI](#)
11. Chiang HH, Wu SJ, Perng JW, Wu BF, Lee TT. The human-in-the-loop design approach to the longitudinal automation system for an intelligent vehicle. *IEEE Trans Syst, Man, Cybern - Part A: Syst Humans* 2010;40:708–20. [DOI](#)
12. Akhegaonkar S, Nouvelière L, Glaser S, Holzmann F. Smart and green ACC: energy and safety optimization strategies for EVs. *IEEE Trans Syst, Man, Cybern: Syst* 2018;48:142–53. [DOI](#)
13. Li S, Li K, Rajamani R, Wang J. Model Predictive Multi-Objective Vehicular Adaptive Cruise Control. *IEEE Trans Contr Syst Technol* 2011;19:556–66. [DOI](#)
14. Hu J, Zhu J, Lei G, Platt G, Dorrell DG. Multi-objective model-predictive control for high-power converters. *IEEE Trans Energy Conv* 2013;28:652–63. [DOI](#)
15. Bageshwar VL, Garrard WL, Rajamani R. Model predictive control of transitional maneuvers for adaptive cruise control vehicles. *IEEE Trans Veh Technol* 2004;53:1573–85. [DOI](#)
16. Li SE, Jia Z, Li K, Cheng B. Fast online computation of a model predictive controller and its application to fuel economy-oriented adaptive cruise control. *IEEE Trans Intell Trans Syst* 2015;16:1199–209. [DOI](#)
17. Corona D, De Schutter B. Adaptive cruise control for a SMART car: a comparison benchmark for MPC-PWA control methods. *IEEE Trans Contr Syst Techn* 2008;16:365–72. [DOI](#)
18. Moser D, Schmied R, Waschl H, del Re L. Flexible spacing adaptive cruise control using stochastic model predictive control. *IEEE Trans Contr Syst Techn* 2018;26:114–27. [DOI](#)
19. Li SE, Guo Q, Xu S, Duan J, Li S, et al. Performance enhanced predictive control for adaptive cruise control system considering road elevation information. *IEEE Trans Intell Veh* 2017;2:150–60. [DOI](#)
20. Gao B, Cai K, Qu T, Hu Y, Chen H. Personalized adaptive cruise control based on online driving style recognition technology and model predictive control. *IEEE Trans Veh Techn* 2020;69:12482–96. [DOI](#)
21. Yang D, Zong G, Su SF. \mathcal{H}_∞ tracking control of uncertain Markovian hybrid switching systems: a fuzzy switching dynamic adaptive control approach. *IEEE Trans Cybern* 2022;52:3111–22. [DOI](#)
22. Xie X, Wei C, Gu Z, Shi K. Relaxed resilient fuzzy stabilization of discrete-time Takagi-Sugeno systems via a higher order time-variant balanced matrix method. *IEEE Trans Fuzzy Syst* 2022;1–1. [DOI](#)

23. Yang W, Feng G, Zhang T. Robust model predictive control for discrete-time Takagi–Sugeno fuzzy systems with structured uncertainties and persistent disturbances. *IEEE Trans Fuzzy Syst* 2014;22:1213–28. [DOI](#)
24. Nguyen AT, Taniguchi T, Eciolaza L, Campos V, Palhares R, et al. Fuzzy control systems: past, present and future. *IEEE Comput Intell Mag* 2019;14:56–68. [DOI](#)
25. Nguyen AT, Rath J, Guerra TM, Palhares R, Zhang H. Robust set-invariance based fuzzy output tracking control for vehicle autonomous driving under uncertain lateral forces and steering constraints. *IEEE Trans Intell Transp Syst* 2021;22:5849–60. [DOI](#)
26. Zhang C, Lam HK, Qiu J, Qi P, Chen Q. Fuzzy-model-based output feedback steering control in autonomous driving subject to actuator constraints. *IEEE Trans Fuzzy Syst* 2021;29:457–70. [DOI](#)
27. Nguyen AT, Sentouh C, Zhang H, Popieul JC. Fuzzy static output feedback control for path following of autonomous vehicles with transient performance improvements. *IEEE Trans Intell Transp Syst* 2020;21:3069–79. [DOI](#)
28. Zhang D, Wang J. A curving ACC system with coordination control of longitudinal car-following and lateral stability. *Veh Syst Dyn* 2012;50:1085–102. [DOI](#)
29. Liu F, Chen Y. Improved model predictive control for cooperative adaptive cruise control subject to actuator delay. In: 2017 Chinese Automation Congress (CAC); 2017. pp. 4747–22. [DOI](#)
30. Zhang H, Zhang X, Wang J. Robust gain-scheduling energy-to-peak control of vehicle lateral dynamics stabilisation. *Veh Syst Dyn* 2014;52:309–40. [DOI](#)
31. Baffet G, Charara A, Dherbomez G. An observer of tire–road forces and friction for active security vehicle systems. *IEEE/ASME Trans Mechatr* 2007;12:651–61. [DOI](#)
32. Rajamani R. Vehicle dynamics and control. Springer Science & Business Media; 2011.
33. Nguyen A, Sentouh C, Zhang H, Popieul J. Fuzzy static output feedback control for path following of autonomous vehicles with transient performance improvements. *IEEE Trans Intell Transp Syst* 2020;21:3069–79. [DOI](#)
34. Yang W, Gao J, Feng G, Zhang TJ. An optimal approach to output-feedback robust model predictive control of LPV systems with disturbances. *Int J Rob Nonl Contr* 2016;26. [DOI](#)
35. Jiang ZP, Wang Y. Input-to-state stability for discrete-time nonlinear systems. *Automatica* 2001;37:857–69. [DOI](#)
36. Magni L, Raimondo DM, Scattolini R. Regional input-to-state stability for nonlinear model predictive control. *IEEE Trans Autom Contr* 2006;51:1548–53. [DOI](#)
37. Xie L, Fu M, de Souza CE. H_∞ control and quadratic stabilization of systems with parameter uncertainty via output feedback. *IEEE Trans Autom Contr* 1992;37:1253–56. [DOI](#)
38. Kothare MV, Balakrishnan V, Morari M. Robust constrained model predictive control using linear matrix inequalities. *Automatica* 1996;32:1361–79. [DOI](#)
39. Costello GA. Theory of wire rope. New York, NY: Springer New York; 1997. [DOI](#)
40. Cheng S, Li L, Guo H, Chen Z, Song P. Longitudinal collision avoidance and lateral stability adaptive control system based on MPC of autonomous vehicles. *IEEE Trans Intell Trans Syst* 2020;21:2376–85. [DOI](#)
41. Lofberg J. YALMIP : a toolbox for modeling and optimization in MATLAB. In: 2004 IEEE International Conference on Robotics and Automation (IEEE Cat. No.04CH37508); 2004. pp. 284–89. [DOI](#)